Laminar flame speeds of lean hydrogen-oxygen-helium mixtures under elevated pressures and temperatures

Combustion and Flame 281 (2025) 114412

Contents lists available at ScienceDirect

Combustion and Flame

journal homepage: www.sciencedirect.com/journal/combustion-and-flame

Laminar flame speeds of lean hydrogen-oxygen-helium mixtures under elevated pressures and temperatures

Hao-Yu Hsieh [a], Andrei N. Lipatnikov [b], Shenqyang (Steven) Shy [a,*]

[a] Department of Mechanical Engineering, National Central University, Taoyuan City 320317, Taiwan
[b] Department of Mechanics and Maritime Sciences, Chalmers University of Technology, Gothenburg SE-412 96, Sweden

ARTICLE INFO

Keywords:
Laminar flame speed
Diffusional-thermal instability
Combustion chemistry and molecular transport
Preheated reactants
Flame stretch rate and curvature

ABSTRACT

Lean H_2/O_2/He laminar spherical flames expanding after spark ignition in the center of a large cruciform burner are investigated using high-speed Schlieren imaging technique. When processing the images, dependencies of equivalent flame radii $<R_f>$ on time are extracted and unperturbed laminar flame speeds S_L^0 are evaluated adopting four state-of-the-art flame-speed-correction methods. The experimental conditions cover lean mixtures at three equivalence ratios ($\phi = 0.3$, 0.45, and 0.6), three pressures ($P = 1$, 3, and 5 atm), and two unburned gas temperatures ($T_u = 300$ and 400 K). Besides, the flame speeds are computed adopting seven state-of-the-art chemical mechanisms. The obtained results show, first, that substitution of nitrogen with helium offers the opportunity to suppress diffusional-thermal instability under the studied conditions and to measure speeds of lean hydrogen laminar flames in wider ranges of equivalence ratios and pressures. Second, substitution of nitrogen with helium results in significantly reducing the influence of non-linear (with respect to flame stretch rate) effects on differences between the observed and unperturbed laminar flame speeds, thus substantially improving accuracy of evaluation of S_L^0 in lean hydrogen mixtures. Third, none of the tested chemical models predict all the experimental data, with differences between measured and computed S_L^0 being particularly large in preheated ($T_u = 400$ K) moderately lean ($\phi = 0.45$) flames under elevated pressures ($P = 3$ and 5 atm). Since chemical kinetic mechanisms of lean hydrogen burning have not yet been tested against experimental data on S_L^0, obtained at $T_u = 400$ K, the present results call for further assessment and development of such models for elevated temperature conditions, which occur, e.g., in piston engines. Fourth, differences between the measured and computed flame speeds could in part be attributed to limitations of the adopted transport models, thus calling for further assessment and development of them also.

1. Introduction

The threat of global warming makes hydrogen a very promising fuel for future combustion engines [1,2]. In particular, green hydrogen, produced through water electrolysis powered by renewable electricity, is an electro-fuel (e-fuel) [3] with zero CO_2 emissions and is increasingly recognized as a key energy carrier for future transportation engines and power generation gas turbines [4]. Besides, operation of such engines and gas turbines in a lean premixed combustion mode can significantly reduce nitrogen oxide emissions [5]. To efficiently take these advantages of hydrogen and to rapidly develop future ultra clean, highly efficient, and safe H_2-fueled piston engines and gas turbines, various research and development (R&D) tools should be used hand in hand. From this perspective, knowledge of basic combustion characteristics of lean hydrogen-air mixtures is strongly required to advance numerical simulations as an efficient tool for R&D of H_2-fueled engines and gas turbines.

The planar, one-dimensional, fully developed laminar flame speed [6] (or unperturbed laminar flame speed S_L^0 for brevity) is one of such combustion characteristics. This speed is difficult to measure in lean hydrogen-air mixtures even under room conditions, with this task being much more challenging under elevated pressures and temperatures associated with burning in piston engines and gas turbines. Unless accurate values of S_L^0 are known under such conditions, chemical mechanisms of hydrogen burning are hardly accepted to be well validated. Accordingly, state-of-the-art models of turbulent flame propagation in engines and gas turbines, which rely often on such chemical mechanisms, do not seem to be a predictive research tool.

* Corresponding author.
E-mail address: sshy@ncu.edu.tw (S.(S. Shy).

https://doi.org/10.1016/j.combustflame.2025.114412
Received 1 February 2025; Received in revised form 8 August 2025; Accepted 9 August 2025
Available online 16 August 2025

The aforesaid difficulty and challenge stem from significant differences in molecular diffusivities of hydrogen, oxygen, and heat. Due to these differences, lean hydrogen-air laminar flames are prone to diffusional-thermal instability [6], which makes flame surface cellular, increases its area, and, hence, impedes accurately measuring S_L^0. While (i) this instability can be suppressed by sufficiently high stretch rates and (ii) there are known various methods [7–11] for extrapolating experimental data on speeds S_L of laminar flames stabilized by stretch rates to the unstretched S_L^0, none of these methods performs well in lean hydrogen-air mixtures. The point is that these methods do not allow accurate prediction of non-linear (with respect to flame stretch rate) effects, which are significant in lean hydrogen-air flames stabilized by stretch rates. For instance, recent complex-chemistry numerical simulations of (i) unperturbed planar flames and (ii) expanding spherical flames have shown that application of any of these methods to the latter flames results in substantially overestimating the extrapolated value of unstretched laminar flame speed when compared to S_L^0 obtained directly from the former flame [8, Fig. 1]. Therefore, experimental data on S_L^0 obtained from sufficiently lean (equivalence ratio $\phi \leq 0.6$) H_2-air mixtures are rare and highly scattered even under room conditions [11, Figs. 27 and 28].

Under elevated pressures, the situation is even worse, because an increase in pressure is known to promote the occurrence of hydrodynamic (Darrieus-Landau, DL) instability [6,12–14]. Specifically, the range of perturbation wavelengths that make the flame unstable is increased with decreasing flame thickness. For instance, a critical flame-kernel radius associated with the appearance of cellular flame surface is decreased with increasing pressure, with all other things being equal [14]. Due to the interaction of DL instability and diffusional-thermal effects, which further expand the range of perturbation wavelengths that make laminar flames unstable, data on S_L^0 of lean hydrogen-air mixtures, measured at $P > 1$ atm, are rare, highly scattered, and limited to quite moderate pressures of few atmospheres [11, Fig. 32a].

Nevertheless, chemical mechanisms of hydrogen burning could be assessed using experimental data on S_L^0, obtained at room or higher pressures, if the influence of diffusional-thermal instability on laminar flame speeds is mitigated by substituting nitrogen in the air with helium. Since molecular diffusivities of H_2 and He are comparable with one another and are significantly higher than molecular diffusivities of O_2 or N_2, lean hydrogen-oxygen-helium mixtures are characterized by Lewis numbers $Le = \alpha/D_{H2}$ sufficiently close to (while slightly smaller than) unity, e.g., see Table 1 in Sect. 2.4. Here, α and D_{H2} are the molecular thermal diffusivity of a lean mixture and the molecular diffusivity of hydrogen in that mixture. Since diffusional-thermal instability of a laminar flame is mitigated by an increase in Le and does not occur if $Le < Le_{cr} < 1$ [6,15–19], this instability is expected to be much less (if any) pronounced in lean H_2-O_2-He mixtures when compared to lean hydrogen-air ones under the same conditions (i.e., the same equivalence ratio ϕ, the same pressure P, and the same unburned gas temperature T_u).

Indeed, Tse et al. [20, Fig. 2a] experimentally demonstrated that surfaces of expanding spherical laminar flames were smooth in a moderately lean ($\phi = 0.7$) H_2-O_2-He mixture at $P = 3$ atm. At $P = 5$ atm, diffusional-thermal instability of such flames was claimed to be suppressed, whereas large-scale wrinkles observed in Schlieren images of the flame surfaces [20, Fig. 2b] were attributed to DL instability, which was known to be controlled by the density ratio, laminar flame speed and thickness [6,12,13], but was not directly affected by differences in molecular transport coefficients of He and N_2. Subsequently, Burke et al. [21] reported values of S_L^0 obtained from expanding spherical H_2-O_2-He flames at $P \leq 10$ atm ($\phi = 0.3$ or 0.5) and $P \leq 25$ atm ($\phi = 0.7$), with $T_u = 295$ K in all these cases. It is worth noting that the influence of He on differences between measured stretched and extrapolated unperturbed laminar flame speeds was not investigated in Refs. [20,21], while substitution of nitrogen with helium is expected not only to suppress diffusional-thermal instability, but also to reduce the magnitude of the non-linear stretch effects [22], which is still poorly predicted in lean hydrogen-air mixtures [8]. Such a reduction is directly associated with an increase in Le and stems also from the opportunity to obtain a larger laminar flame kernel with a smooth surface. Since the magnitude of the non-linear effects is inversely proportional to flame radius [22], they are less pronounced for larger flame kernels..

It is worth noting that due to a high diffusivity of He, dilution of a reacting mixture with it results in increasing laminar flame thickness, thus mitigating DL instability. Accordingly, He was also used for measuring laminar flame speeds under elevated pressures and elevated temperatures in experiments with syngas [23], C1-C4 hydrocarbons [24], or methane-hydrogen blends [25]. However, the influence of He on the magnitude of the non-linear stretch effects was not addressed in the cited papers either.

Despite (i) rapidly growing interest in hydrogen burning in engines and (ii) the high potential of substitution of N_2 with He for measuring S_L^0 of lean hydrogen flames at various pressures [20,21], this substitution method has yet been rarely used for lean burning of H_2. Accordingly, the present work aims at further advancing the method by reporting new experimental data obtained from lean expanding spherical laminar H_2-O_2-He flames at $\phi = 0.3$, 0.45, or 0.6; $P = 1$, 3, or 5 atm; and $T_u = 300$ or 400 K. Specifically, the work aims not only at further demonstrating suppression of diffusional-thermal instability of laminar flames in lean H_2-O_2-He mixtures [20,21], but also at showing that differences in values of S_L^0, calculated by applying different extrapolation techniques [7–11] to measured dependencies of the flame radius R_f on time t, are quite moderate under the studied conditions. In addition, the present experimental data are adopted to assess several state-of-the-art chemical mechanisms of hydrogen burning [26–32], most of that were developed after publication of Refs. [20,21].

In the next section, the adopted experimental and numerical techniques are described. Measured results are reported and discussed in Section 3, where these results are also used to test various chemical

Table 1
Experimental conditions and measured data.

N	Mixture composition	ϕ	X_{He}	P, atm	T_u, K	T_b, K	σ	δ_L^0, mm	Le	Pe
1	$0.6H_2+O_2+5He$	0.30	5.00	5	400	1361	3.24	0.37	0.86	122
2	$0.9H_2+O_2+8.88He$	0.45	8.88	1	300	1211	3.88	1.82	0.92	25
3	$0.9H_2+O_2+8.44He$	0.45	8.44	3	300	1247	4.00	0.95	0.91	47
4	$0.9H_2+O_2+8.44He$	0.45	8.44	5	300	1247	4.00	1.55	0.91	29
5	$0.9H_2+O_2+7.05He$	0.45	7.05	5	300	1383	4.40	0.36	0.88	125
6	$0.9H_2+O_2+8.88He$	0.45	8.88	1	400	1311	3.13	1.30	0.92	35
7	$0.9H_2+O_2+8.44He$	0.45	8.44	3	400	1346	3.22	0.48	0.91	94
8	$0.9H_2+O_2+8.44He$	0.45	8.44	5	400	1346	3.22	0.39	0.91	115
9	$1.2H_2+O_2+8.44He$	0.60	8.44	3	300	1520	4.81	0.33	0.89	136
10	$1.2H_2+O_2+8.44He$	0.60	8.44	5	300	1520	4.81	0.22	0.89	205
11	$1.2H_2+O_2+8.44He$	0.60	8.44	5	400	1618	3.82	0.17	0.89	265

mechanisms. Conclusions are summarized in Section 4.

2. Methods

2.1. Experiments

Centrally-ignited, outwardly-expanding lean H_2/O_2/He laminar spherical flames at three different values of equivalence ratio ($\phi = 0.3$, 0.45, and 0.6) under elevated pressure ($P = 1$, 3, or 5 atm) and temperature ($T_u = 300$ or 400 K) conditions were experimentally investigated using a constant-pressure, constant-temperature, dual-chamber cruciform burner to extract unstretched laminar flame speeds. The high-pressure cruciform burner and its associated diagnostic techniques have been detailed in Refs. [9,33–39]. For completeness, a brief description of the burner follows.

The inner 3D cruciform burner was constructed by a large cylindrical steel pipe placed horizontally with four cylindrical steel pipes perpendicularly aligned and symmetrically welded around the central part of the inner burner, which was resided in a huge outer pressure vessel. The intersecting central volume of the 3D cruciform burner is nearly spherical and has a minimum diameter of about 300 mm. Two identical counter-rotating fans driven by two 10 HP motors together with two identical heated perforated plates are adopted to mix fuel and air before ignition using a pair of cantilevered pin-to-pin spark electrodes. Four large pressure-released valves are symmetrically installed on the top and bottom vertical pipes of the cruciform burner, allowing a spherical laminar premixed flame to expand at a constant pressure condition. For high temperature experiments, there are twenty surface heaters that cover around the cruciform burner alongside the two perforated plate heaters, capable of generating a central uniform constant high-temperature volume of 100×100×100 mm with only 1°C variation for spherical flame speed measurements (please see Refs. [36,38] and [39, Fig. 10] for detailed treatment).

Thus, when compared to quasi-spherical vessels used commonly to explore expanding spherical laminar flames, e.g., see review articles [11, 40], the cruciform burner has three major peculiarities: (i) a big outer chamber, which allows us to safely investigate high-pressure combustion (such a burner design was pioneered by Tse et al. [20]), (ii) four pressure-releasing valves built on the walls of the inner chamber to retain a constant pressure inside it [33], and (iii) the preheating tools [36,38] described above. These peculiarities expand the range of feasible experimental conditions, but weakly (if any) affect precision of measurements of S_L^0. Note that we have used the cruciform burner to measure laminar flame speeds which are consistent with data published by other groups, detailed in Refs. [9,34,36,38].

The experimental procedures to measure laminar flame speeds at 400 K are listed by the following sequence steps. (i) All 20 surface heaters around the surface of the cruciform burner are turned on with a temperature of 160°C for four hours. (ii) The two perforated plate heaters, which are carefully welded by a very long narrow serpentine heating strip in-between arrays of 10 mm holes (see Ref. [36]), are turned on and set to a temperature of 250° C. (iii) The inner cruciform burner is then vacuumed and the appropriate mole fractions of lean H_2/O_2/He mixtures are injected into the heated burner using the partial pressure method to the wanted pressure ($P = 1$, 3, or 5 atm). (iv) A pair of specially designed fans are counter-rotated at a fan frequency of $f =$ 30 Hz for four minutes to well mix the injected gases. Besides, when the two counter-rotating fan-stirred streams pass through the two perforated plate heaters, an efficient turbulent heat convection can be generated allowing a uniform temperature distribution in the experimentation domain. (v) Right after four-minute mixing, the fans are turned off, the turbulence decays rapidly, and the lean H_2/O_2/He mixture is in quiescence within 10 seconds. The mixture is ignited at 10 s after the fan turn-off to assure a uniform temperature distribution in the domain of experimentation during the laminar flame propagation, as detailed in Ref. [36]. (vi) The time evolutions of centrally ignited, outwardly expanding spherical flames are recorded using Schlieren technique by a CMOS high-speed camera (Phantom 711) operated at 10, 000 frames/s with 800×800 pixels. Each Schlieren flame image is processed by adopting the Canny Edge Detection method to obtain an area $A(t)$ enveloped by the flame and its radius $\langle R_f(t)\rangle = [A(t)/\pi]^{0.5}$. The uncertainty in determining the flame radius is estimated to be one pixel, i.e., about 0.16 mm. The measurements are restricted to $\langle R_f(t)\rangle < 50$ mm, i.e., the measured flame radius is always smaller than 1/6 diameter of the chamber to satisfy a widely accepted criterion [41] of spherical flame propagation under constant pressure conditions in a confined volume. Laminar flame speeds reported in the following were obtained by analyzing data measured at 10 mm $< \langle R_f(t)\rangle <$ 45 mm to avoid the ignition influence in the early stage of laminar flame development and confinement effects [41] at large $\langle R_f(t)\rangle$. More detailed information can be found in our previous paper [9].

2.2. Data processing

As discussed in detail elsewhere [7–11], there are known several extrapolation methods for extracting values of S_L^0 by processing $R_f(t)$-curves obtained from expanding spherical flames. Since all these methods are based on perturbation theories that differently treat non-linear (with respect to the perturbation magnitude) effects, differences in values of S_L^0 yielded by different methods characterize importance of the non-linear effects. In the following, we will present results calculated adopting four widely used methods that are based on Activation Energy Asymptotic (AEA) theories of stretched laminar flames with single-step chemistry.

First, some AEA theories [17,22,42,43] consider the case of (i) weak stretch rate, i.e., $\varepsilon \equiv \tau_c^0 \dot{s} \ll 1$, and (ii) small differences between Lewis number and unity and predict the following linear relation

$$S_L = S_L^0 - L\dot{s} + S_L^0 \mathrm{O}(\varepsilon^2) \tag{1}$$

between stretched flame speed S_L and flame stretch rate $\dot{s}$. Here, $\tau_c^0 = \delta_L^0/S_L^0$ and δ_L^0 are unperturbed laminar flame time scale and thickness, respectively, L designates Markstein length, which value depends on the choice of an iso-scalar surface associated with the flame front [22]. Applications of Eq. (1) to processing experimental data obtained from stretched flames were pioneered by Wu and Law [44] who studied steady strained laminar flames. When applied to expanding spherical flames, Eq. (1) is commonly adopted in the following form [22,43]

$$S_{L,b} \equiv \frac{dR_f}{dt} = \sigma S_L^0 - L_b \frac{2}{R_f}\frac{dR_f}{dt} + \sigma S_L^0 \mathrm{O}(\varepsilon^2), \tag{2}$$

where the subscript b refers to quantities measured either with respect to ($S_{L,b}$) or in (L_b) combustion products, the stretch rate $\dot{s} = 2R_f^{-1}dR_f/dt$, and $\sigma = \rho_u/\rho_b$ is the density ratio. As shown by Dowdy et al. [45], Eq. (2) has the following exact analytical solution

$$t = t^* + \frac{1}{S_L^0}\left[R_f - R_f^* + 2L_b \ln\left(\frac{R_f}{R_f^*}\right)\right] = \frac{1}{S_L^0}\left(R_f + 2L_b \ln R_f\right) + t_1^* \tag{3}$$

if small terms on the order of ε^2 are omitted. Here, the time t^* and the flame radius $R_f^* = R_f(t^*)$ correspond to "initial" conditions, which could be associated with any measured point $R_f(t)$, and $t_1^* = t^* - \left(R_f^* + 2L_b \ln R_f^*\right)/S_L^0$. Results obtained from expanding spherical laminar flames were often processed adopting Eq. (3), e.g., see Refs. [7–9,11,45–47].

Second, since non-linear (with respect to $\varepsilon \equiv \tau_c^0 \dot{s} \ll 1$) terms are not retained in Eqs. (1) and (2) [17,22,42,43], the same theoretical result may be rewritten in the following form [22,48]

$$S_{L,b} \equiv \frac{dR_f}{dt} = \sigma S_L^0\left(1 - \frac{2L_b}{R_f}\right) + \sigma S_L^0 \mathrm{O}(\varepsilon^2), \tag{4}$$

which is similar to the seminal hypothesis by Markstein [49]. Equation (4) has the following exact analytical solution [50]

$$t = t^* + \frac{1}{\sigma S_L^0}\left[R_f - R_f^* + 2L_b \ln\left(\frac{R_f - 2L_b}{R_f^* - 2L_b}\right)\right] = \frac{1}{\sigma S_L^0}\left[R_f + 2L_b \ln\left(R_f - 2L_b\right)\right] + t_2^* \tag{5}$$

if small terms on the order of ε^2 are omitted. Here, $t_2^* = t^* - \left[R_f^* + 2L_b \ln\left(R_f^* - 2L_b\right)\right]/S_L^0$. Since the difference between Eqs. (2) and (4)

$$\sigma S_L^0 - L_b \frac{2}{R_f}\frac{dR_f}{dt} - \sigma S_L^0\left(1 - \frac{2L_b}{R_f}\right) = \frac{2L_b}{R_f}\left(\sigma S_L^0 - \frac{dR_f}{dt}\right) = \sigma S_L^0 \mathrm{O}(\varepsilon^2) \tag{6}$$

is of the second order with respect to $\varepsilon \ll 1$, differences between values of S_L^0, obtained using Eqs. (3) and (5), directly characterize magnitude of non-linear (with respect to $\varepsilon \ll 1$) effects.

Another AEA theory of "slowly varying" stretched laminar flames was developed [51,52] by allowing for significant differences in *Le* and unity, but assuming that a product of a small perturbation magnitude and a high normalized activation energy is of unity order. The theory yields

$$\left(\frac{S_{L,b}}{\sigma S_L^0}\right)^2 \ln\left(\frac{S_{L,b}}{\sigma S_L^0}\right)^2 = -\frac{4L_b}{R_f}\frac{S_{L,b}}{\sigma S_L^0} + \frac{2L_b}{S_{L,b}}\frac{dS_{L,b}}{dR_f}, \tag{7}$$

which reduces to both Eq. (2) and Eq. (4) if $\varepsilon \to 0$. Kelley and Law [53] have (i) neglected the last term in Eq. (7) by assuming that expanding spherical flames propagate "in a quasi-steady manner'' and (ii) reported the following exact analytical solution

$$t = t_3^* + \frac{2L_b}{\sigma S_L^0}\left[\int_{\ln\xi^2}^{\infty} \frac{\mathrm{e}^{-z}}{z} dz - \frac{1}{\xi^2 \ln\xi}\right], \xi \ln\xi = -\frac{2L_b}{R_f} \tag{8}$$

to the so-truncated Eq. (7) with $S_{L,b} = dR_f/dt$. Here, the dimensional constant t_3^* is required to satisfy initial conditions. Results obtained from expanding spherical laminar flames were often processed adopting Eq. (8) also, e.g., see Refs. [7–9,11,54–56].

Fourth, Kelley et al. [10] have retained the last term in Eq. (7) and expanded this equation in powers of $2L_b/R_f$ as follows:

$$\frac{S_{L,b}}{\sigma S_L^0}\left\{1 + \frac{2L_b}{R_f} + \left(\frac{2L_b}{R_f}\right)^2 + \frac{2}{3}\left(\frac{2L_b}{R_f}\right)^3 + \mathrm{O}\left[\left(\frac{2L_b}{R_f}\right)^4\right]\right\} = 1. \tag{9}$$

In the limit of $\varepsilon \to 0$, Eq. (9) reduces to Eq. (3), (5), or (7). If the fourth-order terms with respect to $2L_b/R_f \ll 1$ are omitted, the exact analytical solution to Eq. (9) with $S_{L,b} = dR_f/dt$ reads [10]

$$t = \frac{R_f}{\sigma S_L^0}\left\{1 + \frac{2L_b}{R_f}\ln\left(\frac{R_f}{R_{f,4}^*}\right) - \left(\frac{2L_b}{R_f}\right)^2 - \frac{1}{3}\left(\frac{2L_b}{R_f}\right)^3\right\}. \tag{10}$$

Here, the dimensional constant $R_{f,4}^*$ is required to satisfy initial conditions. Results obtained from expanding spherical laminar flames were often processed adopting Eq. (10) also, e.g., see Refs. [8,9,11,57,58].

In the present work, Eqs. (3), (5), (8), and (10) are applied to processing the measured $\langle R_f \rangle(t)$-curves following Ref. [9]. Specifically, an interval of $L_{b,min} < L_b < L_{b,max}$ is divided into 200 equal bins where $L_{b,min} = -15$ mm and $L_{b,max} = 5$ mm. So large values of $L_{b,min}$ and $L_{b,max}$ are set in order for the best-fitting values of L_b to be within the interval $L_{b,min} < L_b < L_{b,max}$ for all processing methods in all cases. Accordingly, results reported in the following are not changed when $L_{b,min}$ is further decreased or $L_{b,max}$ is further increased. Subsequently, for each L_b-bin, (i) the two parameters, i.e., S_L^0 and either t_1^*, t_2^*, and t_3^* in Eqs. (3), (5), and (8), respectively, or $R_{f,4}^*$ in Eq. (10), are determined by applying these linear equations together with the least square fit to the measured $\langle R_f \rangle(t)$-curves and (ii) rms errors of the obtained approximations are calculated as follows:

$$\Delta^2 = \frac{1}{N - j_1 + 1}\sum_{j_1}^{N}\left[\langle R_f \rangle(t_j) - R_F^{an}(t_j)\right]^2. \tag{11}$$

Here, $\langle R_f \rangle(t_j)$ is the measured flame radius, $R_F^{an}(t_j)$ refer to analytical solutions given by Eqs. (3), (5), (8), and (10), N is the total number of measurement instants for a single run, j is the number of each single instant, and $j_1 > 1$ corresponds to the first measurement instant when $\langle R_f \rangle > 10$ mm. Thus, data obtained from small flame kernels ($\langle R_f \rangle < 10$ mm) are omitted to avoid the influence of spark ignition. Finally, a set of L_b, $S_L^0(L_b)$ and $t_n^*(L_b)$ or $R_{f,4}^*(L_b)$ that yield the smallest $\Delta(L_b)$ for $L_{b,min} < L_b < L_{b,max}$ is selected. Such best-fitting values of L_b are always far from the boundaries $L_{b,min}$ and $L_{b,max}$. The reader interested in further details is referred to Ref. [9]. This method is independently applied to each measured $\langle R_f \rangle(t)$-curve, followed by averaging the obtained values of S_L^0 and L_b over five runs.

2.3. Simulations

Stationary, one-dimensional, planar, adiabatic laminar premixed flames are numerically simulated adopting seven state-of-the-art detailed chemical mechanisms [26–32] and running PREMIX module [59] of CHEMKIN-2 package [60]. The numerical grid is automatically refined when a normalized slope of computed variables exceeds 0.02 at any point. The flames are described with common transport equations for mass, momentum, energy, and species concentrations [59] and by the ideal gas state equation. In the studied case, governing partial differential transport equations degenerate to a set of non-linear ordinary differential equations, which are iteratively solved. Molecular mass and heat transfer is described adopting multicomponent transport model [59], with Soret effect being also considered.

2.4. Conditions

Set numbers and experimental conditions are summarized in Table 1, where X_{He} is the number of helium atoms per oxygen molecule in the mixture, T_b is the adiabatic combustion temperature, the laminar flame thickness $\delta_L^0 = (T_b - T_u)/\max|dT/dx|$ has been computed using Konnov's mechanism [32], and Peclet number $Pe = R_f/\delta_L^0$ is estimated for the largest flame radius $R_f = 45$ mm used to evaluate S_L^0. In most cases, $X_{He} > 8$, but the mole fraction of He is reduced in cases 1 and 5 to increase laminar flame speed and to mitigate buoyancy effects, addressed in the next section. In all studied flames, Lewis number is about 0.9, varying from 0.86 in the leanest mixture (case 1) to 0.92 in case 2. Note that the critical Lewis number $Le_{cr} < 1$, which bounds the domain $Le < Le_{cr}$ of diffusional-thermal instability, is not known for the studied mixtures.

3. Results and discussion

3.1. Experimental data

Typical images of the studied H_2/O_2/He laminar flames are shown in Figs. 1-4. Here, a single representative case is selected for each set of conditions. In case 4, the flame shape is significantly deformed due to buoyancy effects, as the laminar flame speed is expected to be low under such conditions. Accordingly, case 4 will not be considered in the rest of the paper. In case 3, large flame kernels are moved up due to buoyancy effects, but the kernel shape remains quasi-spherical, and its surface is

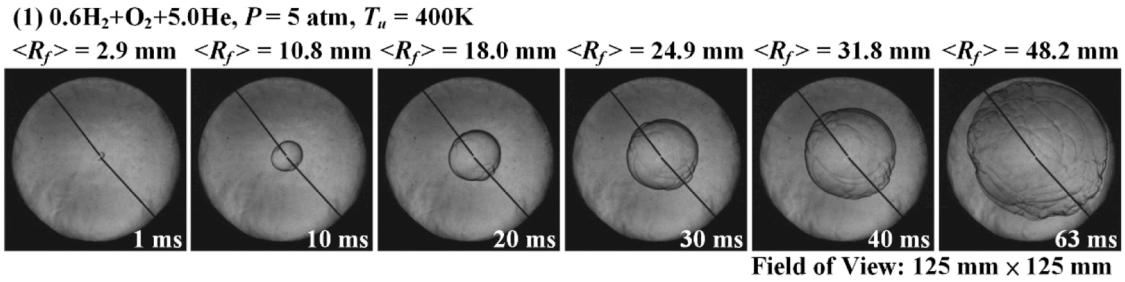

Fig. 1. Typical images of lean H_2/O_2/He laminar flames characterized by $\phi = 0.3$. Case 1: $X_{He} = 5.0$, $P = 5$ atm, $T_u = 400$ K.

still smooth. Accordingly, Eqs. (3), (5), (8), and (10) are applied to processing the raw data obtained in this case and the best-fitting values of S_L^0 and L_b are reported for completeness. Nevertheless, results obtained in case 3 will not be used to draw conclusions summarized in Sect. 4, because the influence of buoyancy on the measured $\langle R_f \rangle(t)$-curves could be substantial. In other cases, the flame surfaces look spherical and smooth, thus indicating that substitution of nitrogen with helium can suppress diffusional-thermal instability and enable accurate measurements of laminar flame speeds in lean hydrogen mixtures under elevated pressures reached in the present work.

In cases 6-8, which are most challenging for chemical models, as discussed in Sect. 3.2, flame surfaces are always smooth, see Fig. 3. However, few large-scale cells are observed in images of flame 1, see Fig. 1, flames 3 and 5, see Fig. 2, flames 9 and 10, see Fig. 4. Following Tse et al. [20], such cells are associated with hydrodynamic instability [6,12,13] that arises due to the density drop across a laminar flame and, consequently, cannot be fully suppressed by substituting N_2 with He (even if this method mitigates the instability [23–25]). To support this association, images of two lean $H_2/O_2/N_2$ laminar flames are reported in Fig. 5 (since combustion of these mixtures were studied in an earlier paper [61], the interested reader is referred to it for further details). As these flames are subject not only to hydrodynamic instability, but also to diffusional-thermal one, much smaller cells (when compared to H_2/O_2/He mixtures) are well seen in Fig. 5, contrary to Figs. 1-4. Significant differences in cell sizes [13,14,22,62] associated with the two instabilities stem from the facts that (i) the range of perturbation length scales capable for triggering laminar flame instabilities is significantly wider for the diffusional-thermal one and (ii) the length scale associated with the peak growth rate of the diffusional-thermal instability is significantly smaller [63, Fig. 3].

While Schlieren images presented in Figs. 1-4 do not reveal appearance of diffusional-thermal instability (contrary to Fig. 5), this qualitative observation requires quantitative support. Typically, the appearance of instability during growth of a spherical flame kernel is indicated by a rapid increase in the observed flame speed $d\langle R_f \rangle/dt$, e.g., see Fig. 3 in Ref. [25] or Figs. 9 and 11 in Ref. [64]. Such an effect is observed in case 1 and is weakly pronounced in case 5, see Supplementary Materials (Figs. S1 and S2). However, the influence of this effect on the values of S_L^0 reported in Table 2 is weak, as will be shown later.

Moreover, since Eqs. (3), (5), (8), and (10) hold for stable laminar flames, deviations between the measured $\langle R_f \rangle(t)$-curves and $R_f^{an}(t)$-curves yielded by these equations can also be adopted to detect the onset of flame instability.

Accordingly, in Fig. 6, raw experimental data on $\langle R_f \rangle(t)$ are compared with fitting curves computed using Eqs. (3) and (5) for each run (different colors) in four cases. The corresponding values of S_L^0 and the Markstein number $Ma_b = L_b/\delta_L$, averaged over five runs, are reported in Table 2, which shows that the magnitudes[1] $|Ma_b|$ are the largest in cases 3, 8, and 11. Accordingly, differences in the measured $S_L(t)$ and the extrapolated S_L^0 are expected to be most pronounced in these three cases, which, consequently, seem to be most challenging. For these reasons, Figs. 6(b), 6(c), and 6(d) show $\langle R_f \rangle(t)$-curves obtained in these three cases, respectively. Figure 6(a) reports results obtained from the leanest flames (case 1), whose surfaces are weakly wrinkled, see Fig. 2. The $\langle R_f \rangle(t)$-curves obtained in other six cases (2, 5-7, 9, and 10) using Eqs. (3) and (5) and the $\langle R_f \rangle(t)$-curves obtained in all cases using Eqs. (8) and (10) are not presented for brevity and because these results are very similar to results plotted in Figs. 6(a), 6(c), and 6(d). The following points are worth noting.

First, there are substantial differences between $\langle R_f \rangle(t)$-curves measured in different runs, e.g., see Fig. 6(c). This phenomenon is well known, e.g., see Fig. 3 in Ref. [65] or Fig. 3(a) in Ref. [66], and could be attributed to random perturbations of the initial kernel shape during spark ignition, variations in energy released by the spark, variations in the equivalence ratio, etc. For instance, the values of S_L^0 obtained in cases 8 and 11 yield the following estimate $dS_L^0/d\phi \approx 600$ cm/s. Accordingly, if $\phi = 0.6 \pm 0.0006$, variations in S_L^0 can be as large as 0.4 cm/s solely due to so-small (0.1%) variations in the equivalence ratio. To mitigate this well-known effect, data obtained from expanding spherical laminar flames are commonly averaged over several runs (five in the present study). This standard method results in quite moderate rms magnitudes of variations in the measured laminar flame speeds, as shown in Table 2. While these rms values are expected to further decrease with increasing number of runs, even the reported rms magnitudes are comparable with uncertainties calculated by Xiouris et al. [23] using a more sophisticated method, see Table 2 in the cited paper.

Second, in all cases presented in Fig. 6 and in other six cases (not shown for brevity), the raw experimental data plotted in symbols are very well fitted using both Eqs. (3) and (5) in each run, see curves plotted in solid and dashed lines, respectively, and note again that results obtained in different runs are plotted using different colors. In all these cases, differences between symbols (experimental data) and solid or dashed line, corresponding to Eq. (3) or (5), respectively, are hardly visible with the naked eye.

To quantify this agreement, the coefficient of determination R^2 was calculated for each run and each fitting method. In all studied cases (with the exception of case 4, which is not analyzed due to strong buoyancy effects), the obtained values of R^2 are very close to unity. For instance, the difference $(1 - R_m^2)$ reported in the right-hand column in Table 2 shows the largest (over five runs and four processing methods)

[1] It is worth stressing that the values of Ma_b are reported for completeness and to select cases characterized by the largest $|Ma_b|$ and, therefore, associated with the most pronounced non-linear effects. The present study aims solely at exploring unperturbed laminar flame speeds, rather than Markstein numbers.

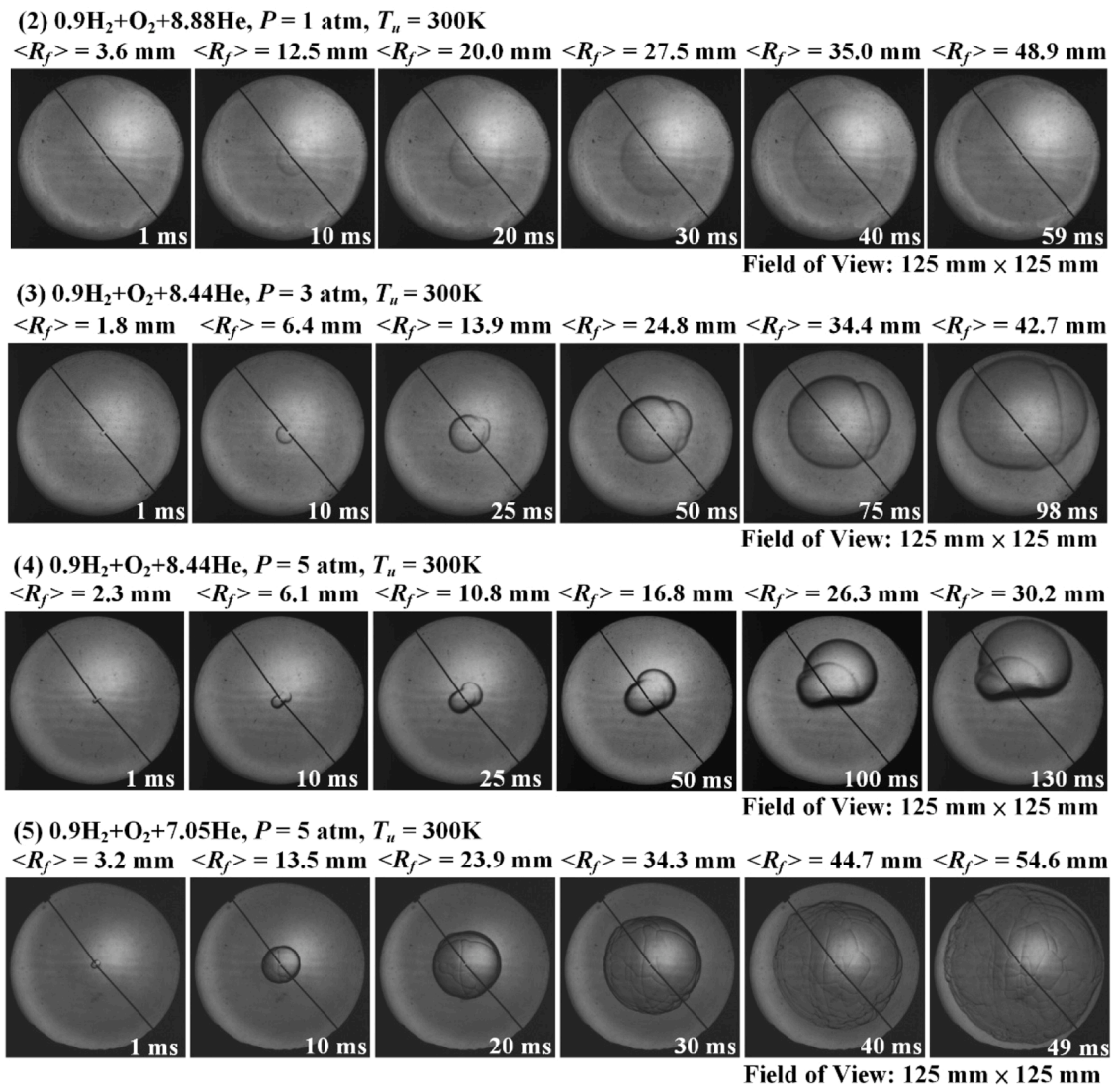

Fig. 2. Typical images of lean H_2/O_2/He laminar flames characterized by $\phi = 0.45$ and $T_u = 300$ K. Case numbers are reported in figure legends.

Table 2
Measured data.

N	S_L^0, cm/s Eq. (3)	S_L^0, cm/s Eq. (5)	S_L^0, cm/s Eq. (8)	S_L^0, cm/s Eq. (10)	ΔS_L^0, cm/s	Ma_b Eq. (3)	Ma_b Eq. (5)	Ma_b Eq. (8)	Ma_b Eq. (10)	$1 - R_m^2$
1	21.8±0.8	21.8±0.7	21.9±0.8	21.8±0.8	0.17	0.3±0.5	0.2±0.5	0.2±0.5	0.2±0.5	10^{-4}
2	19±1	19±1	19±1	19±1	0.35	-0.5±0.1	-0.6±0.2	-0.6±0.2	-0.6±0.2	10^{-4}
3	8.1±0.5	7.3±0.4	6.8±0.3	7.6±0.4	1.7	-2.8±0.2	-5.4±0.6	-8.3±1	4.5±0.4	$6{\cdot}10^{-4}$
5	24.1±0.5	24.0±0.5	24.0±0.6	24.0±0.5	0.22	0.06±0.8	±0.9	±0.9	±0.9	$3{\cdot}10^{-5}$
6	59±1	59±1	59±1	59±1	0.58	0.3±0.8	0.3±0.6	0.2±0.8	0.3±0.6	$7{\cdot}10^{-6}$
7	24.9±0.7	24.8±0.7	24.8±0.6	24.8±0.7	0.23	-1.4±0.3	-1.7±0.4	-1.8±0.5	-1.7±0.4	10^{-5}
8	17.2±0.9	17.0±0.8	17.0±0.7	17.0±0.8	0.67	-3.0±0.8	-4±1	-4.5±1.5	-4±1	$5{\cdot}10^{-5}$
9	66±2	66±2	66±2	66±2	0.41	-1.3±0.2	-1.5±0.3	-1.5±0.3	-1.5±0.3	$2{\cdot}10^{-6}$
10	44±2	44±2	45±2	45±2	0.26	-0.5±0.9	-0.5±0.9	-0.3±1	-0.5±0.9	$2{\cdot}10^{-6}$
11	106.8±0.6	106.9±0.7	106.4±0.7	106.9±0.7	1.0	2.0±0.6	1.9±0.6	1.7±0.4	1.9±0.6	$5{\cdot}10^{-6}$

values of $(1 - R_m^2)$, i.e., in all other 19 data sets (for a single mixture), R^2 is closer to unity. These numbers clearly show excellent quantitative agreement between the experimental data and the curves yielded by Eqs. (3), (5), (8), and (10). Since these equations hold for stable laminar flames and do not allow for buoyancy effects, the extremely small differences $(1 - R_m^2)$ prove that the influence of laminar flame instabilities on the measured $\langle R_f \rangle(t)$-curves was weak in all ten considered cases. This weak influence of DL instability on the studied flames is consistent with moderate values of Peclet numbers, reported in Table 1. For comparison, the critical values of Peclet number, associated with significant influence of DL instability on laminar flames, are typically higher, e.g., larger than 350 [67, Fig. 11], larger than 1000 [68, Fig. 5], or as large as 1660 [25].

To further support the weak influence of DL instability on the reported values of S_L^0, the same data were processed using a truncated range of flame radii, i.e., $\langle R_f(t)\rangle < 35$ mm. Since DL instability appears when flame kernels are sufficiently large, this truncation method is expected to yield smaller values of S_L^0 (if DL instability plays a role) when compared to the data reported in Table 2 and obtained at $\langle R_f(t)\rangle < 45$ mm. In case 1, such differences are noted, i.e., the values of S_L^0 obtained using Eqs. (3), (5), (8), and (10) at $\langle R_f(t)\rangle < 35$ mm are equal to 20.7 ±0.6, 20.6±0.6, 20.6±0.6, and 20.6±0.6, respectively. However, these differences are small, i.e., the counterpart flame speeds reported in Table 2 are larger by approximately 5%, with the uncertainty intervals overlapping. Such differences are smaller than 2.5% in case 5 and are significantly smaller in cases 2 and 6-11. These numbers are consistent with figures presented in Supplementary Materials, which show that a weak increase in $d\langle R_f\rangle/dt$ with further decreasing small stretch rates is also observed in case 5, but such an effect is not detected in other cases.

It is also of interest that $(1-R_m^2) \ll 1$ even for mixture 3, thus implying a minor effect of buoyancy on S_L^0 reported in Table 2. Nevertheless, it is worth noting that $(1-R_m^2)$ is significantly larger for this mixture when compared to other nine mixtures, thus implying some influence of buoyancy on the reported flame speed in case 3.

Third, the curves presented in Figs. 6(a), 6(c), and 6(d), as well as curves obtained in the other six cases (not shown) look like straight lines, thus, implying that non-linear effects, i.e., non-linear terms omitted in Eq. (2), (4), (7), or (9), play a minor role under the present experimental conditions. In cases 1, 2, and 5-11, this minor role is quantified using small values of the largest (over five runs and four methods for every single mixture) difference ΔS_L^0 between the speeds S_L^0, yielded by Eqs. (3), (5), (8), and (10), see the sixth column in Table 2. These largest differences characterize data-processing uncertainties analyzed by Xiouris et al. [23] using other methods under different conditions. Such uncertainties are also characterized by $1-R_m^2$, see the rightest column in Table 2.

The small values of ΔS_L^0 and $1-R_m^2$ show that the substitution of nitrogen with helium offers the opportunity to overcome another fundamental difficulty in measuring laminar flame speeds of lean hydrogen-air mixtures, i.e., significant influence of the non-linear effects [8] on the difference in $S_L(t)$ and S_L^0. These findings can be explained using AEA theories of stretched laminar premixed flames. According to such theories, [10,15–18,22,42,43,51,52], (i) magnitude of non-linear effects is increased by $|L_b|$, e.g., non-linear terms in Eqs. (6) and (9) are directly proportional to L_b, and (ii) $L_b < 0$ in lean hydrogen-air flames ($Le < 1$) due to a negative term that is proportional to $Ze(Le-1)$, where Ze is Zel'dovich number. Therefore, when N_2 is substituted with He, (i) Lewis number is increased, i.e., goes to unity, (ii) the magnitudes of the negative terms $(Le-1)$ and $Ze(Le-1)$ are decreased, and, consequently, (iii) Markstein length $L_b < 0$ goes to zero, i.e., the magnitude of L_b is decreased. As a result, the non-linear effects are less pronounced for smaller $|L_b|$. Moreover, since the range of radii of stable flames (i.e., flames whose surfaces are smooth) is substantially increased due to substitution of N_2 with He, the ratio of $|L_b|/R_f$ is further decreased. Consequently, the non-linear effects are mitigated.

It is worth noting, however, that the case design adopted in the present work does not guarantee that such non-linear effects play a minor role under other conditions, e.g., leaner mixtures or higher pressures. To resolve the problem, S_L^0 could be evaluated by (i) running unsteady complex-chemistry numerical simulations of expanding spherical flames and (ii) applying the computed $S_{L,b}(\dot{s})$-curves to processing experimental data presented in the same form, as proposed by Wang et al. [69], see also more recent papers [23–25]. However, this advanced method has not yet been applied to lean ($\phi \le 0.6$) hydrogen flames to the best of the present authors' knowledge. In cases 1, 2, and 5-11, this method is not required, because the non-linear effects are reduced due to the case design.

Nevertheless, the discussed non-linear effects appear to play a role in case 3. Indeed, first, the measured $\langle R_f\rangle(t)$-curves seem to have a weakly pronounced non-linear shape, see Fig. 6(b). Second, the values of S_L^0, yielded by Eqs. (3) and (8), are substantially (about 17 %) different in this case. Third, ΔS_L^0 is significantly larger than in other cases. Fourth, the values of Ma_b yielded by Eqs. (3), (5), (8), and (10) are significantly different, whereas intervals of scatter of Ma_b overlap for all these equations in cases 1, 2, and 5-11. Fifth, dependencies of the observed flame speed $\sigma^{-1}dR_f/dt$ on stretch rate, computed using Eqs. (5), (8), and (10), are weakly non-linear in case 3, see Fig. 7(a). In other cases, the counterpart curves are almost linear, e.g., see Figs. 7(b)-7(d), which show results obtained from mixtures 7, 8, and 11. These three cases are selected, because they are characterized by three next-to-the-largest $|Ma_b|$ in Table 2. Accordingly, in six other mixtures, the non-linear effects are less pronounced (not shown for brevity).

The emphasized features of case 3 are (at least in part) are associated with buoyancy effects, which are indicated by asymmetry of images of the flame surface, see Fig. 2b. Buoyancy effects seem to play a role in this case, because laminar flame speed obtained in case 3 is significantly smaller than the speeds of other explored flames (with the exception of case 4). Accordingly, Richardson number $Ri = (1-\sigma^{-1})gR_f/S_L^2$, estimated for the largest flame radius $\langle R_f\rangle = 45$ mm and invoking S_L^0 reported in the second column in Table 2, is as large as 50 in case 3. In other cases (with the exception of case 4), $Ri < 10$. Here, g is gravitational acceleration. It is worth noting that while high values of Ri are commonly associated with significant buoyancy effects, a critical value of Ri that bounds a domain of importance of such effects is not known for spherically expanding laminar flames. Since (i) measurements of laminar flame speeds are routinely performed for moderately lean ($\phi = 0.75$) methane-air mixture under room conditions using spherical bombs [11, Fig. 34] and (ii) $Ri = 11$ under such conditions if $R_f = 45$ mm, the aforementioned critical value of Ri is expected to be substantially larger than 10.

In summary, while the substitution of N_2 with He does not allow us to resolve all issues associated with measurements of speeds of lean hydrogen laminar flames, this method does offer the opportunity to measure S_L^0 at substantially low equivalence ratios and under elevated pressures. Such data are useful for assessing various detailed chemical mechanisms of hydrogen combustion, as illustrated in the next subsection.

3.2. Assessment of various chemical mechanisms

Values of S_L^0 measured in the present work are compared with the speeds S_L^0 computed using seven detailed chemical mechanisms in Table 3, where

$$\epsilon = \left[S_{L,\mathrm{sim}}^0 - S_{L,\mathrm{exp}}^0\right] \Big/ S_{L,\mathrm{exp}}^0 \tag{12}$$

designates relative difference between the measured $S_{L,\mathrm{exp}}^0$ and the computed $S_{L,\mathrm{sim}}^0$. Note that the results yielded by mechanisms of Metcalfe et al. [30] and Goswami et al. [31] are reported in the same column, because these results are identical for all H_2/O_2/He mixtures addressed in the present work.

Table 3 shows that none of the used chemical mechanisms can accurately predict the measured data, with the relative difference ϵ being large in many cases. Differences between S_L^0 computed using different mechanisms are also large for certain H_2/O_2/He mixtures, e.g., cf. results yielded by mechanisms [29] and [30]. At the same temperature $T_u = 400$ K (or $T_u = 300$ K), the largest (for various pressures) relative difference ϵ between experimental and numerical data is smaller for $\phi = 0.60$ when compared to $\phi = 0.30$ ($\phi = 0.45$, respectively).

In cases 7 and 8 ($\phi = 0.45$, $T_u = 400$ K, $P = 3$ and 5 atm, respec-

Table 3
Laminar flame speeds computed for the present experimental conditions.

N	exp	simulations											
		[26]		[27]		[28]		[29]		[30,31]		[32]	
	S_L^0, cm/s	S_L^0, cm/s	ϵ	S_L^0, cm/s	ϵ	S_L^0, cm/s	ϵ	S_L^0, cm/s	ϵ	S_L^0, cm/s	ϵ	S_L^0, cm/s	ϵ
1	21.8	25.3	0.16	21.7	0.004	25.4	0.16	31.5	0.44	21.4	0.02	27.9	0.28
2	19	26.4	0.40	23.3	0.23	27.9	0.47	31.2	0.64	23.2	0.22	26.4	0.40
3	8.1	10.5	0.29	8.17	0.009	12.2	0.51	14.9	0.84	9.17	0.13	12.9	0.59
5	24.0	22.4	0.07	19.8	0.18	22.6	0.06	27.4	0.14	19.6	0.18	23.4	0.03
6	59	72.7	0.23	66.6	0.13	73.9	0.25	80.1	0.36	64.7	0.10	68.6	0.16
7	25	48.3	0.93	43.5	0.74	49.8	0.99	57.1	1.28	42.7	0.71	48.8	0.95
8	17.2	28.2	0.64	24.4	0.42	30.1	0.75	36.1	1.10	24.7	0.44	31.4	0.82
9	66	66.7	0.01	63.8	0.03	65.2	0.01	72.6	0.10	61.3	0.07	62.0	0.06
10	44	52.6	0.20	50.3	0.14	51.1	0.16	58.7	0.33	48.1	0.09	49.8	0.13
11	107	116	0.08	112	0.05	112	0.05	125	0.17	107	0.0	108	0.009

tively), values of ϵ reported in Table 3 are significantly larger than the rms scatter of the measured data or the data-processing uncertainties ΔS_L^0, see Table 2. Therefore, the used mechanisms poorly predict the present experimental data obtained from preheated lean H_2/O_2/He mixture under elevated pressures. Specifically, the mechanisms result in significantly overestimating S_L^0. These differences between measured data and computed flame speeds cannot be attributed to experimental uncertainties, because, in cases 7 and 8, Eqs. (3), (7), (8), and (10) fit the measured data very well ($R^2 \cong 1$) and yield close averaged values of S_L^0, with the largest difference ΔS_L^0 being small. These differences cannot be attributed to instability and buoyancy effects, because (i) typical flame images presented in Fig. 3 show smooth spherical flame surfaces, but do not indicate convection of the flame kernels, and (ii) observed flame speeds $S_{L,b}$ monotonically decrease with increasing $\langle R_f \rangle$, see Supplemental Materials, cases 7 and 8. Moreover, if flame instability played a role, the measured flame speeds would be overestimated, contrary to results reported in Table 3. This negative test outcome could be attributed to eventual limitations of these mechanisms and seems to be in line with recent findings by Han et al. [70, p. 9] who recommended updating "temperature dependence of the rate expressions" for certain reactions included in most chemical mechanisms of hydrogen burning. Besides, the large values of ϵ could be attributed to eventual limitations of the commonly used transport models for He-containing mixtures, as discussed below.

As reviewed by Brown et al. [71] and by Konnov et al. [11], majority of chemical models adopted in simulations of laminar flames, including models developed in Refs. [26–31], involve Sandia transport database [72] created using 12-6 Lennard-Jones potential to calculate diffusion coefficients. Limitations of this approach are known since the work by Paul and Warnatz [73], can result in underestimation of molecular diffusion coefficients [74], and are of importance for prediction extinction phenomena [75]. Therefore, binary diffusion coefficients are often computed from first principles adopting quantum scattering calculations, as reviewed by Brown et al. [71]. For combustion

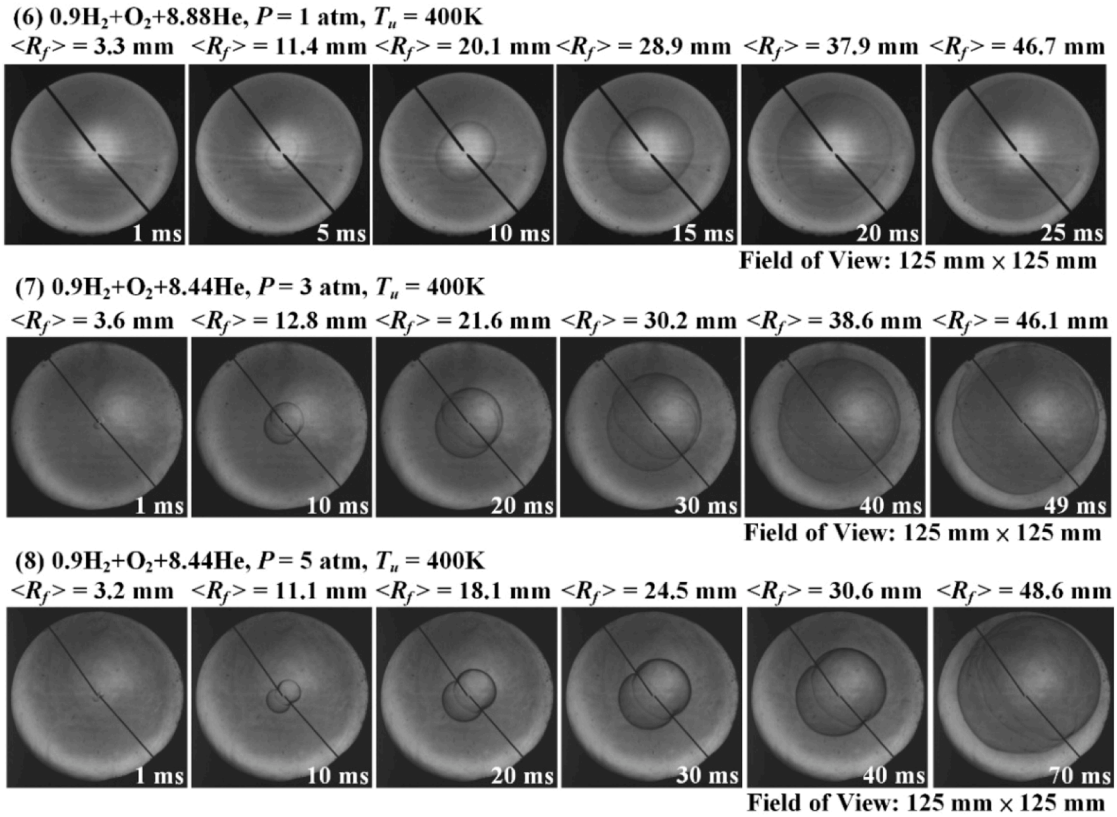

Fig. 3. Typical images of lean H_2/O_2/He laminar flames characterized by $\phi = 0.45$ and $T_u = 400$ K. Case numbers are reported in figure legends.

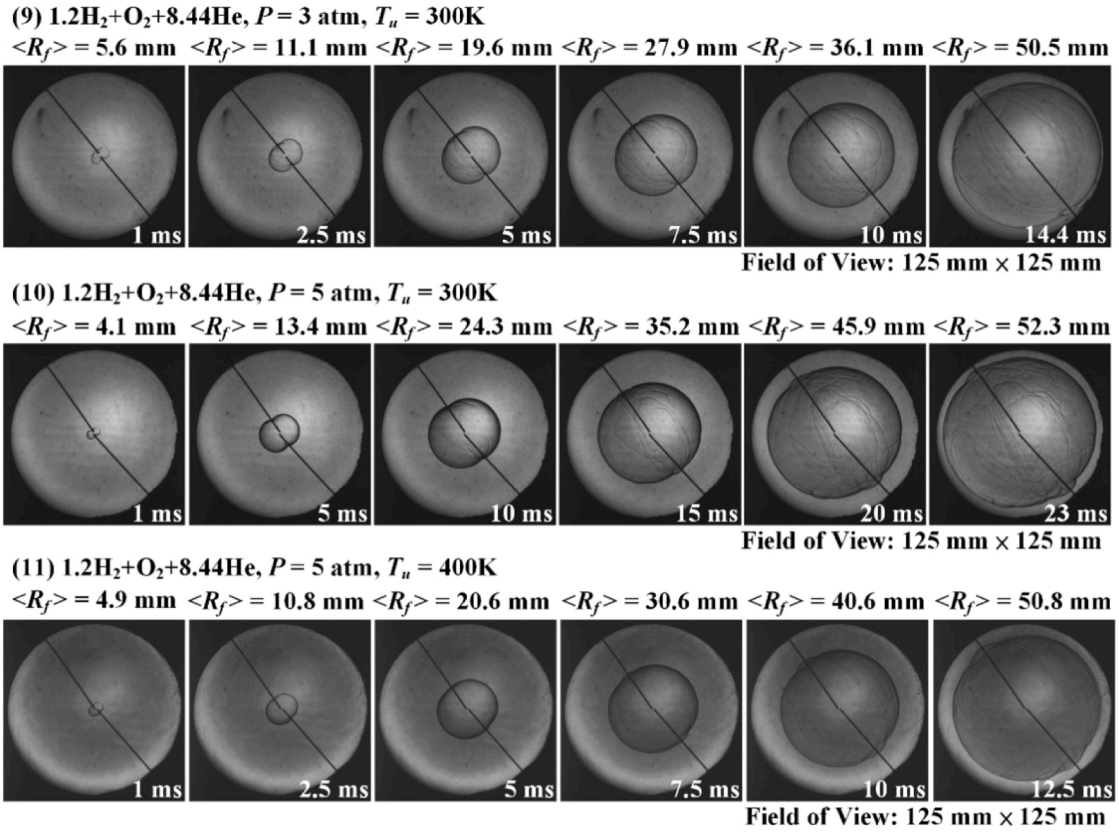

Fig. 4. Typical images of lean H_2/O_2/He laminar flames characterized by $\phi = 0.60$. Case numbers are reported in figure legends.

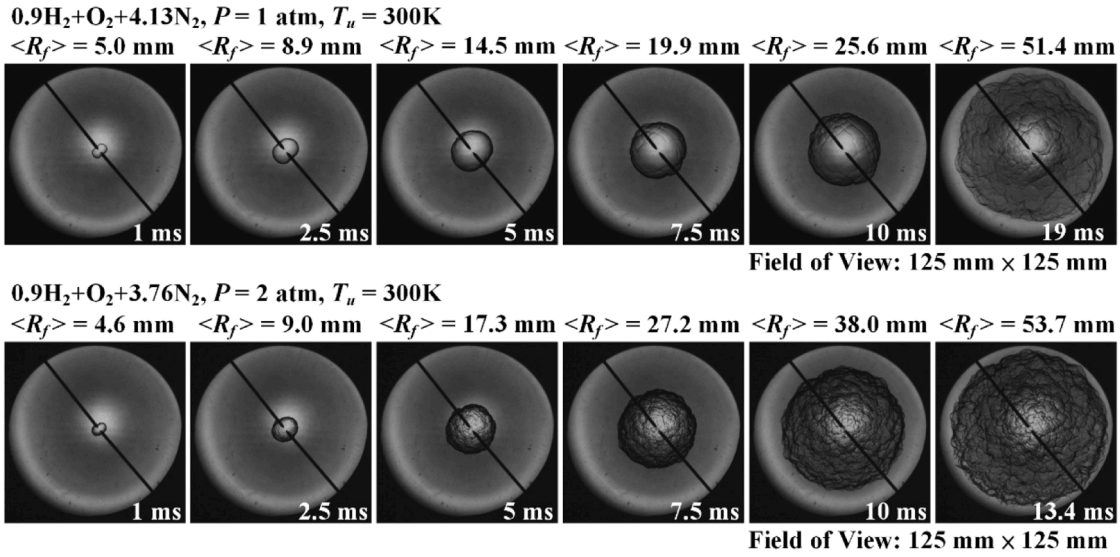

Fig. 5. Typical images of lean $H_2/O_2/N_2$ laminar flames characterized by $\phi = 0.45$ and $T_u = 300$ K. Mixture composition and pressure are specified in figure legends.

applications, Jasper et al. [76,77] created a new transport property database by calculating parameters of 12-6 Lennard-Jones potential from accurate full-dimensional intermolecular potentials and using several first-principles theoretical methods. This database is adopted by Konnov in his chemical model [32]. Thus, the entire chemical models from Refs. [26–31] and from Ref. [32] involve two different transport databases from Refs. [72,77], respectively. Accordingly, extra simulations were performed by combining chemical mechanisms and thermodynamic databases from Refs. [26–31] with the transport database from Refs. [32,77]. Obtained results are reported in Table 4, where an asterisk is added after reference numbers to indicate that the model is changed.

Comparison of results presented in Tables 3 and 4 shows that such a change of the transport database results in reducing (i) S_L^0 in all studied cases and (ii) the difference ϵ in majority of cases. Nevertheless, ϵ is still high in case 7 or 8, i.e., at $T_u = 400$ K, $\phi = 0.45$, and $P = 3$ or 5 atm, respectively. It is worth stressing that this exercise does not aim at recommending the adopted change of transport database. Even if results

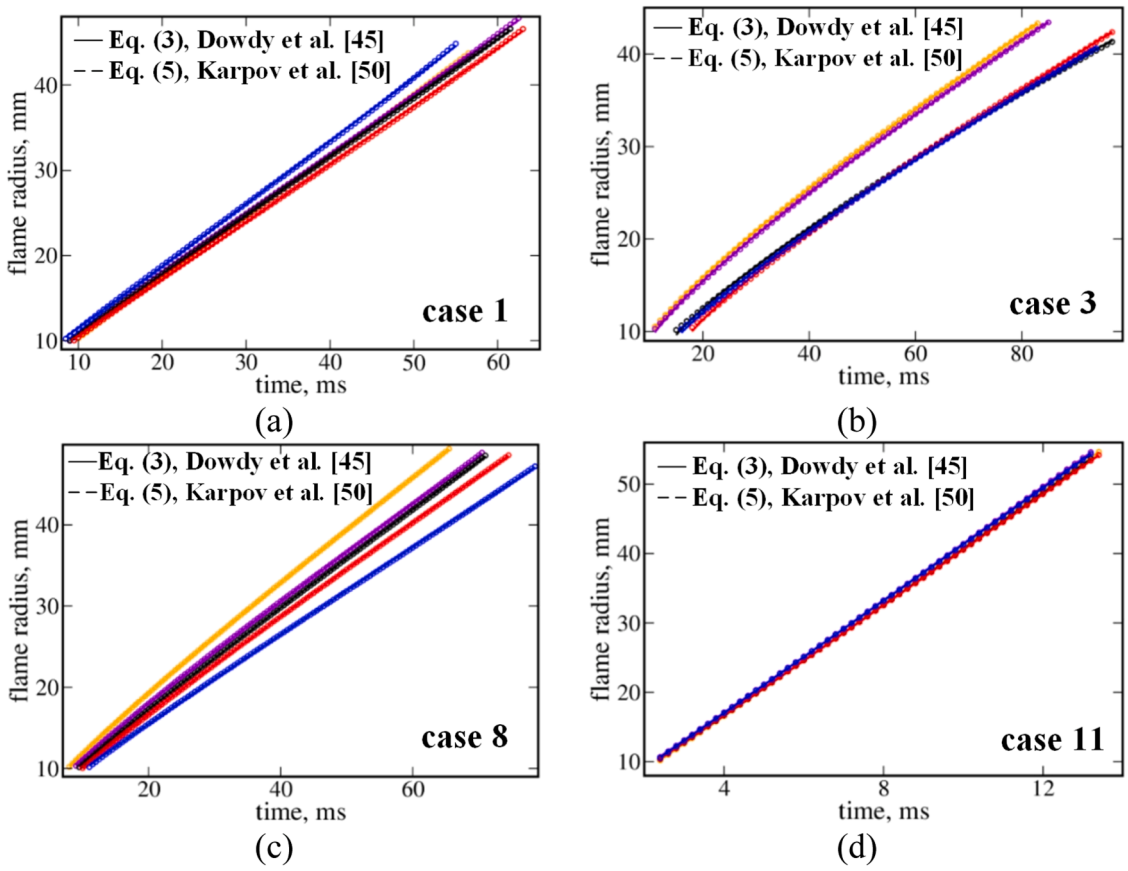

Fig. 6. Dependence of measured flame radius on time counted from spark ignition. Symbols show experimental data. Error bars are not visible, because they are smaller than symbols (as small as 0.16 mm, see Sect. 2.1). Results obtained in five different runs are shown in five different colors.

computed for lean H_2/O_2/He mixtures are improved, the trend could be opposite for other mixtures. Therefore, the discussed exercise aims solely at demonstrating that the reported difference between measured and computed data can stem not only from eventual limitations of chemical mechanisms but also from eventual limitations of transport models, which could play a more important role in lean H_2/O_2/He flames when compared to hydrogen-air ones. This seems to be a disadvantage of substitution of nitrogen with helium for assessing chemical mechanisms of hydrogen burning against laminar flame speeds measured in lean mixtures. The issue requires further studies.

Finally, it is worth noting that the tested chemical models [26–32] predict experimental data by Burke et al. [21] better when compared to the present experimental data, see Tables 5 and 6. Specifically, models by Metcalfe et al. [30], by Goswami et al. [31], and by Burke et al. [27] yield small ϵ in most cases. However, the conditions of the present measurements and experiments by Burke et al. [21] are substantially different. First, preheated mixtures were not investigated by Burke et al. [21], whereas the largest disagreement between the present experimental data and numerical results is observed at $T_u = 400$ K. Second, the ratio X_{He} of mole fractions of helium and oxygen in reactants was significantly smaller in all measurements by Burke et al. [21] when compared to all present cases with the exception of case 5, whose conditions ($\phi = 0.45$, $X_{He} = 7.05$, $P = 5$ atm, and $T_u = 300$ K) are comparable with the conditions of case H ($\phi = 0.50$, $X_{He} = 7.75$, $P = 5$ atm, and $T_u = 295$ K) in the study by Burke et al. [21]. In these two cases, the measured values of S_L^0 are also comparable, i.e., 24.7 cm/s in case 5 and 23.1 cm/s in case H. Despite a lower equivalence ratio, the former flame speed could be larger due to a smaller X_{He}. Moreover, numerical results yielded by four mechanisms [26,28,29,32] agree with the present data (case 5) better, i.e., ϵ is smaller, whereas other mechanisms [27,30,31] agree better with the data obtained by Burke et al. [21] from flame H. Therefore, the two sets of data seem to be consistent, as far as they can be compared.

4. Conclusions

Unperturbed laminar flame speeds S_L^0 are evaluated using four methods to process $\langle R_f \rangle$-curves obtained from expanding spherical laminar lean ($\phi = 0.30$, 0.45, and 0.60) H_2/O_2/He flames at three different pressures ($P = 1$, 3, and 5 atm) and two different temperatures ($T_u = 300$ and 400 K). To the best of the authors' knowledge, S_L^0 has not yet been measured in so lean preheated hydrogen flames. Moreover, laminar flame speeds under conditions listed in Table 1 are computed adopting seven state-of-the-art chemical mechanisms. The following results are worth emphasizing.

First, in line with earlier experiments by Tse et al. [20] and Burke et al. [21], substitution of nitrogen with helium is shown to offer the opportunity to suppress diffusional-thermal instability under the studied conditions and to measure speeds of lean hydrogen laminar flames in wider ranges of equivalence ratios and pressures.

Second, substitution of nitrogen with helium is also shown to offer the opportunity to significantly reduce the influence of non-linear (with respect to flame stretch rate) effects on differences between the observed and unperturbed laminar flame speeds, thus, substantially improving accuracy of evaluation of S_L^0 in lean hydrogen mixtures.

Third, none of the tested chemical models can predict all the experimental data, with differences between measured and computed S_L^0 being particularly large in preheated ($T_u = 400$ K) moderately lean ($\phi = 0.45$) flames under elevated pressures ($P = 3$ and 5 atm). Since chemical kinetic mechanisms of lean hydrogen burning have not yet been tested against experimental data on S_L^0, obtained at $T_u = 400$ K, the present

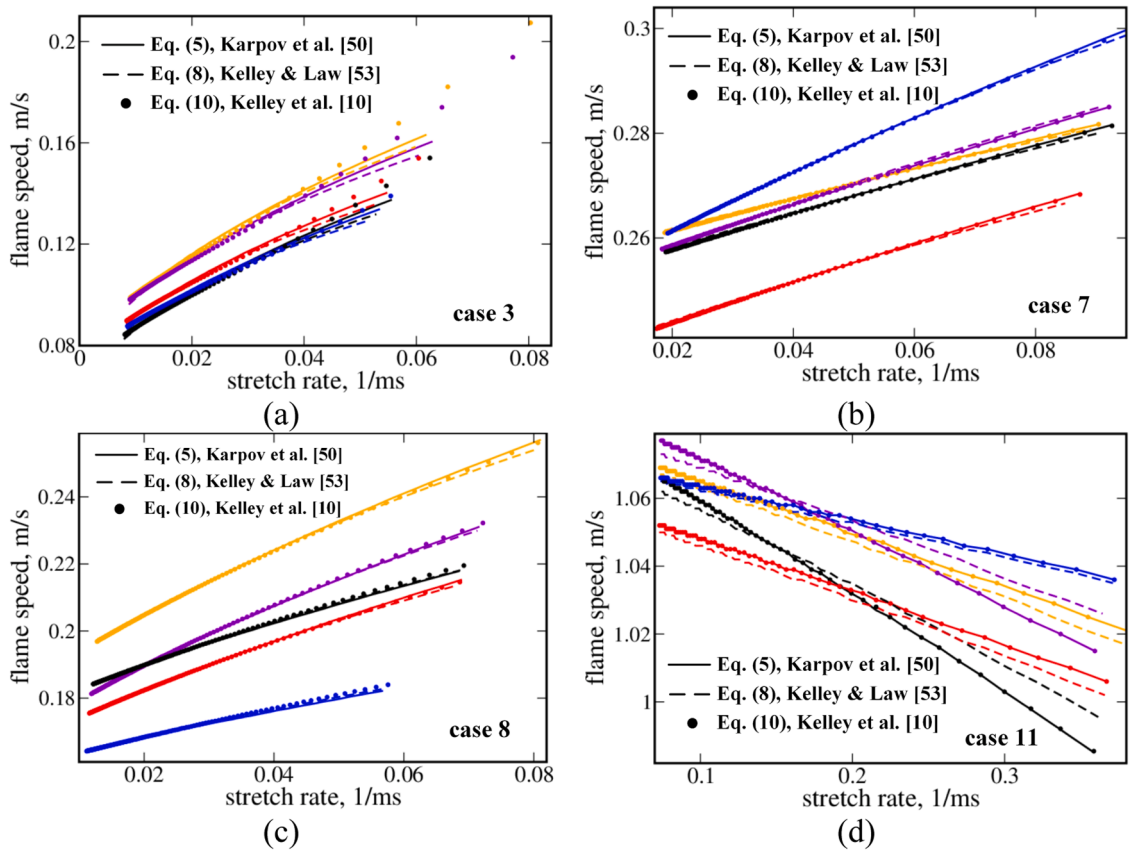

Fig. 7. Dependence of flame speed $\sigma^{-1}dR_f/dt$ on stretch rate. Five different colors correspond to five repeated runs.

Table 4
Laminar flame speeds computed for the present experimental conditions by changing transport model parameter database.

N	exp	simulations									
		[26]*		[27]*		[28]*		[29]*		[30]* or [31]*	
	S_L^0, cm/s	S_L^0, cm/s	ϵ	S_L^0, cm/s	ϵ	S_L^0, cm/s	ϵ	S_L^0, cm/s	ϵ	S_L^0, cm/s	ϵ
1	21.8	21.0	0.03	18.1	0.17	21.0	0.03	26.3	0.21	17.8	0.19
2	19	22.4	0.18	19.7	0.03	23.9	0.26	26.8	0.41	19.7	0.04
3	8.1	9.02	0.11	7.27	0.10	10.5	0.30	13.1	0.61	8.01	0.01
5	24.7	18.6	0.25	16.3	0.34	18.8	0.24	23.0	0.07	16.2	0.34
6	59	64.2	0.09	58.6	0.007	65.4	0.11	71.5	0.21	56.7	0.04
7	25	41.0	0.64	36.8	0.47	42.7	0.71	49.2	0.97	36.1	0.45
8	17.2	23.1	0.34	20.0	0.16	25.0	0.45	30.1	0.75	20.2	0.18
9	66	58.8	0.11	56.2	0.15	57.5	0.13	64.6	0.02	53.9	0.18
10	44	45.5	0.03	43.3	0.02	44.3	0.01	51.2	0.16	41.4	0.06
11	108	103	0.05	99.7	0.08	99.4	0.08	112	0.04	94.6	0.12

Table 5
Conditions of experiments by Burke et al. [21].

Case	A	B	C	D	E	F	G	H	I	J	K	L	M
ϕ	0.30	0.30	0.30	0.30	0.30	0.50	0.50	0.50	0.50	0.50	0.50	0.50	0.50
X_{He}	4.0	4.0	4.0	4.0	3.0	7.75	7.75	7.75	7.75	7.75	6.09	6.09	6.09
P, atm	1	2.5	5	10	5	1	2.5	5	7.5	10	1	5	10

results call for further assessment and development of such models for elevated temperature conditions, which occur, e.g., in piston engines and gas turbines.

Fourth, the difference between the measured and computed flame speeds could (in part) be attributed to limitations of the adopted transport models, thus calling for further assessment and development of them.

Finally, as suggested by one of anonymous Reviewers, numerical simulations run using varying chemical mechanisms can provide a valuable baseline to assess the performance and validity of extrapolation models. Since the flame speed-stretch rate relationship is fundamentally governed by physical transport phenomena, such simulations can offer a controlled framework to directly probe these dependencies, deserving further studies.

Table 6
Laminar flame speeds computed for conditions of experiments by Burke et al. [21].

	exp	Simulations											
		[26]		[27]		[28]		[29]		[30,31]		[32]	
	S_L^0, cm/s	S_L^0, cm/s	ϵ	S_L^0, cm/s	ϵ	S_L^0, cm/s	ϵ	S_L^0, cm/s	ϵ	S_L^0, cm/s	ϵ	S_L^0, cm/s	ϵ
A	55.4	62.0	0.12	56.6	0.02	61.6	0.11	66.5	0.20	54.9	0.01	57.7	0.04
B	34.0	41.3	0.21	37.3	0.1	40.0	0.18	46.2	0.36	35.8	0.05	39.6	0.16
C	17.3	22.2	0.28	19.6	0.13	20.6	0.19	25.9	0.50	18.7	0.08	22.4	0.29
D	5.9	6.98	0.18	5.52	0.07	5.6	0.04	7.84	0.33	4.87	0.18	6.31	0.07
E	58.2	64.7	0.11	61.0	0.04	59.2	0.02	69.4	0.19	56.2	0.03	59.4	0.02
F	61.0	63.7	0.04	59.4	0.03	63.3	0.04	68.0	0.11	57.7	0.05	58.8	0.04
G	37.9	45.7	0.21	42.3	0.11	45.5	0.20	51.4	0.36	41.0	0.08	43.6	0.15
H	23.1	27.5	0.19	24.9	0.08	26.8	0.16	32.8	0.42	24.3	0.05	27.8	0.20
I	15.0	16.3	0.08	14.0	0.07	16.5	0.10	20.4	0.36	13.8	0.08	17.6	0.17
J	8.2	9.50	0.16	7.51	0.08	9.62	0.17	12.1	0.47	7.06	0.14	10.5	0.28
K	105	107	0.02	102	0.03	106	0.01	111	0.05	98.7	0.06	98.0	0.07
L	64.3	71.3	0.11	68.4	0.06	68.2	0.06	77.5	0.21	64.8	0.01	66.3	0.03
M	40.1	46.3	0.16	44.3	0.11	43.1	0.07	51.4	0.28	40.6	0.01	44.2	0.10

Novelty and significance statement

The novelty of this work consists of (i) presenting new experimental data on speeds of lean hydrogen/oxygen/helium laminar flames, with such data being never reported for so lean preheated mixtures, (ii) demonstrating that substitution of nitrogen with helium offers the opportunity to suppress diffusional-thermal instability, to significantly reduce magnitude of non-linear effects, and, hence, to measure unstretched laminar flame speeds in substantially wider ranges of low equivalence ratios and pressures, (iii) showing that the state-of-the-art chemical models poorly predict the new experimental data obtained from preheated lean hydrogen mixtures. The significance of this work is that (i) the found disagreement between experimental and numerical data calls for further development of chemical models of lean hydrogen burning at elevated temperatures and pressures and (ii) the reported new data can be used for testing future chemical models.

CRediT authorship contribution statement

Hao-Yu Hsieh: Visualization, Investigation, Formal analysis, Data curation. **Andrei N. Lipatnikov:** Writing – review & editing, Writing – original draft, Investigation, Formal analysis, Data curation, Conceptualization. **Shenqyang (Steven) Shy:** Writing – review & editing, Writing – original draft, Supervision, Methodology, Investigation, Funding acquisition, Formal analysis, Data curation.

Declaration of competing interest

The authors declare that they have no known competing financial interests or personal relationships that could have appeared to influence the work reported in this paper.

Acknowledgements

SSS gratefully acknowledges the financial support by National Science and Technology Council, Taiwan under grants (NSTC 112-2221-E-008-093-MY2; MOST 111-2221-E-008-053-MY3). ANL gratefully acknowledges the financial support by Swedish Research Council (grant 2023-04407).

Supplementary materials

Supplementary material associated with this article can be found, in the online version, at doi:10.1016/j.combustflame.2025.114412.

References

[1] A. Dreizler, H. Pitsch, V. Scherer, C. Schulz, J. Janicka, The role of combustion science and technology in low and zero impact energy transformation processes, Appl. Energy Combust. Sci. 7 (2021) 100040.
[2] F. Ueckerdt, C. Bauer, A. Dirnaichner, J. Everall, R. Sacchi, G. Luderer, Potential and risks of hydrogen-based e-fuels in climate change mitigation, Nat. Clim. Change 11 (2021) 384–393.
[3] S. Brynolf, J. Hansson, J.E. Anderson, I.R. Skov, T.J. Wallington, M. Grahn, A. D. Korberg, E. Malmgren, M. Taljegård, Review of electrofuel feasibility-prospects for road, ocean, and air transport, Prog. Energy 4 (2022) 042007.
[4] F. Kourougianni, A. Arsalis, A.V. Olympios, G. Yiasoumas, C. Konstantinou, P. Papanastasiou, G.E. Georghiou, A comprehensive review of green hydrogen energy systems, Renew. Energy 231 (2024) 120911.
[5] S. Hayashi, H. Yamada, M. Makida, Extending low-NOx operating range of a lean premixed-prevaporized gas turbine combustor by reaction of secondary mixtures injected into primary stage burned gas, Proc. Combust. Inst. 30 (2005) 2903–2911.
[6] Ya.B. Zel'dovich, G.I. Barenblatt, V.B. Librovich, G.M. Makhviladze, The Mathematical Theory of Combustion and Explosions, Consultants Bureau, New York, 1985.
[7] Z. Chen, On the extraction of laminar flame speed and Markstein length from outwardly propagating spherical flames, Combust. Flame 158 (2011) 291–300.
[8] F. Wu, W. Liang, Z. Chen, Y. Ju, C.K. Law, Uncertainty in stretch extrapolation of laminar flame speed from expanding spherical flames, Proc. Combust. Inst. 35 (2015) 663–670.
[9] A.N. Lipatnikov, S.S. Shy, W.Y. Li, Experimental assessment of various methods of determination of laminar flame speed in experiments with expanding spherical flames with positive Markstein lengths, Combust. Flame 162 (2015) 2840–2854.
[10] A.P. Kelley, J.K. Bechtold, C.K. Law, Premixed flame propagation in a confining vessel with weak pressure rise, J. Fluid Mech. 691 (2012) 26–51.
[11] A.A. Konnov, A. Mohammad, V.R. Kishore, N. Kim, C. Prathap, S. Kumar, A comprehensive review of measurements and data analysis of laminar burning velocities for various fuel+air mixtures, Prog. Energy Combust. Sci. 68 (2018) 197–267.
[12] L.D. Landau, E.M. Lifshitz, Fluid Mechanics, Pergamon, Oxford, 1987.
[13] C.K. Law, Combustion Physics, Cambridge University Press, Cambridge, UK, 2006.
[14] D. Bradley, Instabilities and flame speeds in large-scale premixed gaseous explosions, Phil. Trans. R. Soc. London 357 (1999) 3567–3581.
[15] G.I. Sivashinsky, Diffusional-thermal theory of cellular flames, Combust. Sci. and Technol. 15 (1977) 137–146.
[16] P. Clavin, F.A. Williams, Effects of molecular diffusion and of thermal expansion on the structure and dynamics of premixed flames in turbulent flows of large scale and low intensity, J. Fluid Mech. 116 (1982) 251–282.
[17] M. Matalon, B.J. Matkowsky, Flames as gas dynamic discontinuities, J. Fluid Mech. 124 (1982) 239–260.
[18] F.A. Williams, Combustion theory, Benjamin/Cummings, Menlo Park, CA, 1985.
[19] M.A. Liberman, Combustion Physics. Flames, Detonations, Explosions, Astrophysical Combustion and Inertial Confinement Fusion, Springer, Switzerland, 2021.
[20] S.D. Tse, D.L. Zhu, C.K. Law, Morphology and burning rates of expanding spherical flames in H_2/O_2/inert mixtures up to 60 atmospheres, Proc. Combust. Inst. 28 (2000) 1793–1800.
[21] M.P. Burke, F.L. Dryer, Y. Ju, Assessment of kinetic modeling for lean $H_2/CH_4/O_2$/diluent flames at high pressures, Proc. Combust. Inst. 33 (2011) 905–912.
[22] P. Clavin, Dynamical behavior of premixed flame fronts in laminar and turbulent flows, Prog. Energy Combust. Sci. 11 (1985) 1–59.
[23] C. Xiouris, T. Ye, J. Jayachandran, F.N. Egolfopoulos, Laminar flame speeds under engine-relevant conditions: Uncertainty quantification and minimization in spherically expanding flame experiments, Combust. Flame 163 (2016) 270–283.

[24] A. Movaghar, R. Lawson, F.N. Egolfopoulos, Confined spherically expanding flame method for measuring laminar flame speeds: Revisiting the assumptions and application to C1-C4 hydrocarbon flames, Combust. Flame 212 (2020) 79–92.
[25] K. Van, A. Hu, J.Z. Fang, T.K. Bera, A.A. Aradi, S.K. Jain, F.N. Egolfopoulos, Quantitative studies of instabilities of confined spherically expanding flames: Application to flame propagation and autoignition of natural gas blends with hydrogen at engine-relevant conditions, Combust. Flame 274 (2025) 114009.
[26] J. Li, Z. Zhao, A. Kazakov, F.L. Dryer, An updated comprehensive kinetic model of hydrogen combustion, Int. J. Chem. Kinetics 36 (2004) 566–575.
[27] M.P. Burke, M. Chaos, Y. Ju, F.L. Dryer, S.J. Klippenstein, Comprehensive H_2/O_2 kinetic model for high-pressure combustion, Int. J. Chem. Kinet. 44 (2012) 444–474.
[28] E. Ranzi, A. Frassoldati, R. Grana, A. Cuoci, T. Faravelli, A.P. Kelley, C.K. Law, Hierarchical and comparative kinetic modeling of laminar flame speeds of hydrocarbon and oxygenated fuels, Prog. Energy Combust. Sci. 38 (2012) 468–501.
[29] A. Kéromnès, W.K. Metcalfe, K.A. Heufer, N. Donohoe, A.K. Das, C.-J. Sung, J. Herzler, C. Naumann, P. Griebel, O. Mathieu, M.C. Krejci, E.L. Petersen, W. J. Pitz, H.J. Curran, An experimental and detailed chemical kinetic modeling study of hydrogen and syngas mixture oxidation at elevated pressures, Combust. Flame 160 (2013) 995–1011.
[30] W.K. Metcalfe, S.M. Burke, S.S. Ahmed, H.J. Curran, A hierarchical and comparative kinetic modeling study of C1-C2 hydrocarbon and oxygenated fuels, Int. J. Chem. Kinet. 45 (2013) 638–675.
[31] M. Goswami, R.J.M. Bastiaans, A.A. Konnov, L.P.H. de Goey, Laminar burning velocity of lean H_2-CO mixtures at elevated pressure using the heat flux method, Int. J. Hydrogen Energy 39 (2014) 1485–1498.
[32] A.A. Konnov, Yet another kinetic mechanism for hydrogen combustion, Combust. Flame 203 (2019) 14–22.
[33] C.C. Liu, S.S. Shy, H.C. Chen, M.W. Peng, On interaction of centrally-ignited, outwardly-propagating premixed flames with fully-developed isotropic turbulence at elevated pressure, Proc. Combust. Inst. 33 (2011) 1293–1299.
[34] C.C. Liu, S.S. Shy, M.W. Peng, C.W. Chiu, Y.C. Dong, High-pressure burning velocities measurements for centrally-ignited premixed methane/air flames interacting with intense near-isotropic turbulence at constant Reynolds numbers, Combust. Flame 159 (2012) 2608–2619.
[35] S.S. Shy, C.C. Liu, J.Y. Lin, L.L. Chen, A.N. Lipatnikov, S.I. Yang, Correlations of high-pressure lean methane and syngas turbulent burning velocities: Effects of turbulent Reynolds, Damköhler, and Karlovitz numbers, Proc. Combust. Inst. 35 (2015) 1509–1516.
[36] L.J. Jiang, S.S. Shy, W.Y. Li, H.M. Huang, M.T. Nguyen, High-temperature, high-pressure burning velocities of expanding turbulent premixed flames and their comparison with Bunsen-type flames, Combust. Flame 172 (2016) 173–182.
[37] M.T. Nguyen, D.W. Yu, S.S. Shy, General correlations of high pressure turbulent burning velocities with the consideration of Lewis number effect, Proc. Combust. Inst. 37 (2019) 2391–2398.
[38] S. Yamada, D. Shimokuri, S.S. Shy, T. Yatsufusa, Y. Shinji, Y.R. Chen, Y.C. Liao, T. Endo, Y. Nou, F. Saito, Y. Sakai, A. Miyoshi, Measurements and simulations of ignition delay times and laminar flame speeds of nonane isomers, Combust. Flame 227 (2021) 283–295.
[39] S.S. Shy, Spark ignition transitions in premixed turbulent combustion, Prog. Energy Combust. Sci. 98 (2023) 101099.
[40] F.N. Egolfopoulos, N. Hansen, Y. Ju, K. Kohse-Höinghaus, C.K. Law, F. Qi, Advances and challenges in laminar flame experiments and implications for combustion chemistry, Prog. Energy Combust. Sci. 43 (2014) 36–67.
[41] M.P. Burke, Z. Chen, Y. Ju, F.L. Dryer, Effect of cylindrical confinement on the determination of laminar flame speeds using outwardly propagating flames, Combust. Flame 156 (2009) 771–779.
[42] P. Pelcé, P. Clavin, Influence of hydrodynamics and diffusion upon the stability limits of laminar premixed flames, J. Fluid Mech. 124 (1982) 219–237.
[43] M.L. Frankel, G.J. Sivashinsky, On effects due to thermal expansion and Lewis number in spherical flame propagation, Combust. Sci. and Technol. 31 (1983) 131–138.
[44] C.K. Wu, C.K. Law, On the determination of laminar flame speeds from stretched flames, Proc. Combust. Inst. 20 (1984) 1941–1949.
[45] D.R. Dowdy, D.B. Smith, S.C. Taylor, A. Williams, The use of expanding spherical flames to determine burning velocities and stretch effects in hydrogen-air mixtures, Proc. Combust. Inst. 23 (1990) 325–332.
[46] T. Tahtouh, F. Halter, C. Mounaïm-Rousselle, Nonlinear effects of stretch on the flame front propagation, Combust. Flame 156 (2009) 1735–1743.
[47] V.V. Zamashchikov, V.A. Alekseev, A.A. Konnov, Laminar burning velocities of rich near-limiting flames of hydrogen, Int. J. Hydrogen Energy 39 (2014) 1874–1881.
[48] A.N. Lipatnikov, Some issues of using Markstein number for modeling premixed turbulent combustion, Combust. Sci. and Technol. 119 (1996) 131–154.
[49] G.H. Markstein, Experimental and theoretical studies of flame front stability, J. Aeronaut. Sci. 18 (1951) 199–220.
[50] V.P. Karpov, A.N. Lipatnikov, P. Wolanskii, Finding the Markstein number using the measurements of expanding spherical laminar flames, Combust. Flame 109 (1997) 436–448.
[51] M. Matalon, J.K. Bechtold, Spherically expanding flames, in: Proceedings of 1987 ASME/JSME Thermal Engineering Joint Conference 1, 1987, pp. 95–101.
[52] P.D. Ronney, G.I. Sivashinsky, A theoretical study of propagation and extinction of nonsteady spherical flame fronts, SIAM J. Appl. Math. 49 (1989) 1029–1046.
[53] A.P. Kelley, C.K. Law, Nonlinear effects in the extraction of laminar flame speed from expanding spherical flames, Combust. Flame 156 (2009) 1844–1851.
[54] A.P. Kelley, W. Liu, Y.X. Xin, A.J. Smallbone, C.K. Law, Laminar flame speeds, non-premixed stagnation ignition, and reduced mechanisms in the oxidation of iso-octane, Proc. Combust. Inst. 33 (2011) 501–508.
[55] J.X. Zhou, M. Cordier, C. Mounaïm-Rousselle, F. Foucher, Experimental estimate of the laminar burning velocity of iso-octane in oxygen-enriched and CO_2-diluted air, Combust. Flame 158 (2011) 2375–2383.
[56] B. Galmiche, F. Halter, F. Foucher, Effects of high pressure, high temperature and dilution on laminar burning velocities and Markstein lengths of iso-octane/air mixtures, Combust. Flame 159 (2012) 3286–3299.
[57] F. Wu, C.K. Law, An experimental and mechanistic study on the laminar flame speed, Markstein length and flame chemistry of the butanol isomers, Combust. Flame 160 (2013) 2744–2756.
[58] J. Jayachandran, A. Lefebvre, R. Zhao, F. Halter, E. Varea, B. Renou, F. N. Egolfopoulos, A study of propagation of spherically expanding and counterflow laminar flames using direct measurements and numerical simulations, Proc. Combust. Inst. 35 (2015) 695–702.
[59] R.J. Kee, J.F. Crcar, M.D. Smooke, J.A. Miller, PREMIX: A FORTRAN program for modeling steady laminar one-dimensional premixed flames, Report No. SAND-89-8249, Sandia National Laboratories, 1985.
[60] R.J. Kee, F.M. Rupley, J.A. Miller, CHEMKIN-II: A FORTRAN chemical kinetics package for the analysis of gas-phase chemical kinetics, Report No. SAND-89-8009, Sandia National Laboratories, 1989.
[61] H.Y. Hsieh, S.M. Mousavi, A.N. Lipatnikov, S.S. Shy, Experimental study of the influence of Lewis number, laminar flame thickness, temperature, and pressure on turbulent flame speed using hydrogen and methane fuels, Proc. Combust. Inst. 40 (2024) 105752.
[62] V.P. Karpov, Cellular flame structure under conditions of a constant-volume bomb and its relationship with vibratory combustion, Combust. Expl. Shock Waves 1 (1965) 39–42.
[63] L. Berger, M. Grinberg, B. Jürgens, P.E. Lapenna, F. Creta, A. Attili, H. Pitsch, Flame fingers and interactions of hydrodynamic and thermodiffusive instabilities in laminar lean hydrogen flames, Proc. Combust. Inst. 39 (2023) 1525–1534.
[64] D. Bradley, R.A. Hicks, M. Lawes, C.G.W. Sheppard, R. Woolley, The measurement of laminar burning velocities and Markstein numbers for iso-octane-air and iso-octane-n-heptane-air mixtures at elevated temperatures and pressures in an explosion bomb, Combust. Flame 115 (1998) 126–144.
[65] A.A. Burluka, A.M.T. El-Dein Hussin, C.G.W. Sheppard, K. Liu, V. Sanderson, Turbulent combustion of hydrogen-CO mixtures, Flow Turbulence Combust 86 (2011) 735–749.
[66] S. Wang, A.M. Elbaz, O.Z. Arab, W.L. Roberts, Turbulent flame speed measurement of NH_3/H_2/air and CH_4/air flames and a numerical case study of NO emission in a constant volume combustion chamber (C.V.C.C.), Fuel 332 (2023) 126152.
[67] D. Bradley, C.G.W. Sheppard, R. Woolley, D.A. Greenhalgh, R.D. Lockett, The development and structure of flame instabilities and cellularity at low Markstein number explosions, Combust. Flame 122 (2000) 195–209.
[68] C.R. Bauwens, J.M. Bergthorson, S.B. Dorofeev, Experimental study of spherical-flame acceleration mechanisms in large-scale propane–air flames, Proc. Combust. Inst. 35 (2015) 2059–2066.
[69] Y.L. Wang, A.T. Holley, C. Ji, F.N. Egolfopoulos, T.T. Tsotsis, H. Curran, Propagation and extinction of premixed dimethyl-ether/air flames, Proc. Combust. Inst. 32 (2009) 1035–1042.
[70] X. Han, W. Weng, Y. He, Z. Wang, A.A. Konnov, Experimental and kinetic modelling study on the laminar burning velocities of ultra-lean n-heptane flames at atmospheric pressure, Combust. Flame 268 (2024) 113613.
[71] N.J. Brown, L.A. Bastien, P.N. Price, Transport properties for combustion modeling, Prog. Energy Combust. Sci. 37 (2011) 565–582.
[72] R.J. Kee, G. Dixon-Lewis, J. Warnatz, M.E. Coltrin, J.A. Miller, A Fortran computer code package for the evaluation of gas-phase multicomponent transport properties, Report No. SAND86-8246, Sandia National Laboratories, 1986.
[73] P. Paul, J. Warnatz, A re-evaluation of the means used to calculate transport properties of reacting flows, Proc. Combust. Inst. 27 (1998) 495–504.
[74] P. Middha, B. Yang, H. Wang, A first-principle calculation of the binary diffusion coefficients pertinent to kinetic modeling of hydrogen/oxygen/helium flames, Proc. Combust. Inst. 29 (2002) 1361–1369.
[75] Y. Dong, A.T. Holley, M.G. Andac, F.N. Egolfopoulos, S.G. Davis, P. Middha, H. Wang, Extinction of premixed H_2/air flames: chemical kinetics and molecular diffusion effects, Combust. Flame 142 (2005) 374–387.
[76] A.W. Jasper, E. Kamarchik, J.A. Miller, S.J. Klippenstein, First-principles binary diffusion coefficients for H, H_2, and four normal alkanes + N_2, J. Chem. Phys. 141 (2014) 124313.
[77] A.W. Jasper, J.A. Miller, Lennard-Jones parameters for combustion and chemical kinetics modeling from full-dimensional intermolecular potentials, Combust. Flame 161 (2014) 101–110.